Fractional Fourier Transform Based Channel Estimation in Underwater Acoustic Communications

Jeffrey Shao*, Chenyang Zhang*, Yixuan Xie*, Deepak Mishra*, Yue Rong†, Peng Chen†, and Jinhong Yuan*
*School of Electrical Engineering and Telecommunications, *University of New South Wales (UNSW)*, Sydney, Australia
†School of Electrical Engineering, Computing and Mathematical Sciences, *Curtin University,* Perth, Australia

***Abstract*—Underwater communications have severe channel distortions which can greatly affect its performance. This paper proposes a novel approach for estimating channel parameters (multipath delay and Doppler scaling) for underwater acoustic channels. The method is a Fractional Fourier Transform (FrFT) based approach with linear frequency-modulated (chirp) signals as a pilot. Innovation lies in the receiver design, where a 2D array is formed by performing a scan of FrFTs on the received signal. Key point detection algorithms are exploited to extract distinct X-shaped features in a 2D array, allowing for simultaneous estimation of both channel delay and Doppler parameters for all multipath components. The novel approach avoids the costly iterative process used in existing algorithms, which calculates Doppler scaling for one path per iteration. Simulation results show that the proposed algorithm is capable of estimating channel parameters in a severely time-delayed and Doppler-scaled multipath channel. The algorithm achieved a $\pm 0.1\%$ estimation accuracy with Doppler scaling factors ranging between 0.95 to 1.05. Multipath delay was estimated to within ± 2ms for delays ranging from 0 to 0.2 seconds.**

I. Introduction

In recent years, there has been significant research and experimentation in the field of underwater acoustic (UWA) communications. Ocean research and pollution monitoring have become increasingly important in the scientific sector, whereas offshore monitoring and autonomous vehicles are gaining popularity in the commercial and military sectors. These applications require greater reliability, higher data rates, and greater range capabilities, but UWA channels present unique challenges that are not seen in terrestrial electromagnetic communications. Due to the slow speed of UWA signals relative to the movement of the transmitter/receiver, the Doppler scaling phenomena is three orders of magnitude larger than in terrestrial systems [1]. Moreover, UWA channels are severely time spread with significant multipath delay which necessitates innovative receiver algorithms.

A. State of the Art

Three predominant technologies exist within underwater communications: acoustic, optical, and electromagnetic (EM) [2]. Although EM and optical communications benefit from higher data rates both are unsuitable for long range communication. For the former, propagation is limited to 1 to 200 metres by the conductive nature of saline water, especially in oceans [3]. For the latter, even greater attenuation occurs due to water absorption and scattering from floating particles resulting in a 2 to 100 metre range [2]. In contrast, UWA communications operate up to 120 km [2] making it the preferred technology for long distance applications.

Current UWA communication research dealing with Doppler estimation either assumes all multipaths to have common Doppler scaling or, treats all multipaths as having statistically independent Doppler scaling. The assumption of common Doppler scaling benefits from overall simplicity. However, in applications such as underwater autonomous vehicles, and high data rate communication the emerging multipath dependent Doppler estimation has proven more useful [4]. Nonetheless, common Doppler estimation is more advanced in its research maturity so it serves as a point of comparison in this paper.

The most well established common Doppler estimation approach is the block-based correlation approach outlined in [5]. The idea is to form blocks of data by prepending and appending a pilot signal with strong autocorrelation property around the data. At the receiver, matched filtering produces two peaks whose time difference directly calculates Doppler scaling. In addition to its common Doppler limitations explained above, the block-based approach suffers from high-bit-error rates when the coherence time of the channel drops within the block duration. Another well researched common Doppler estimator is the correlation based method [6]. In this method Doppler scaled copies of the transmitted signal are correlated with the received signal through a correlator bank. The scaling factor corresponding to the maximum peak response is chosen as the Doppler estimate. One major drawback is that computational complexity scales with precision as the estimate resolution depends on the number of correlators. In general, both of the above methods are simple and in principle are used to estimate the Doppler scaling for the dominant path exclusively.

Within the multipath dependent Doppler estimation methods there is relatively less literature but one promising approach stands out. In [7], a scan of FrFTs is performed to estimate the Doppler scaling for the most dominant multipath component. The delay of the dominant component is then found by cross-correlating the received signal with the previously found multipath component. The dominant multipath is then subtracted from the received signal, and the process is repeated for the next most dominant multipath. Iterations occur until the desired number of multipaths have been estimated.

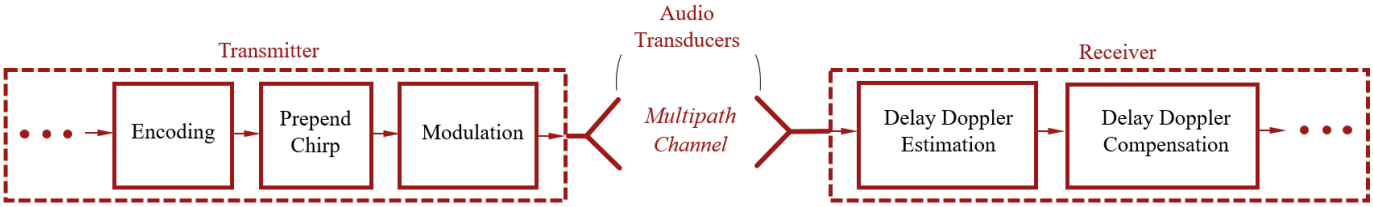

Fig. 1. Block diagram of overall transmitter receiver structure. *Prepend Chirp* and *Delay Doppler Estimation* blocks are newly introduced

B. Motivation and Contribution

This paper presents a multipath Doppler and delay estimation method motivated by long range, high speed, and high data rate application areas. The common Doppler assumption is not made, in favour of a multipath dependent Doppler model that is more useful in such areas. Contributions include:

- Simultaneous estimation of parameters Doppler scaling and multipath delay for all multipaths. This includes the joint estimation of Doppler scaling and multipath delay. This lies in contrast to the successive estimation process of existing methods.
- Greater efficiency in the estimation process.
- Use of key point detection as a technique in the estimation process for the first time in underwater telecommunications.

II. System Model

A. UWA Communication System

Doppler scaling constitutes the most severe and non-linear distortions in an underwater communication system. Thus, it is imperative for the estimation and compensation step to be first in the receiver processing and occur prior to demodulation. The introduction of the chirp pilot signal takes place in the transmitter prior to modulation. Both of these steps are depicted in Fig. 1.

B. UWA Channel and Signal Model

In the current literature there are a few accepted definitions of Doppler scaling. In this paper, Doppler scaling will be denoted by a and refers to the compression or expansion of signals in the time domain. It is defined as

$$a = 1 + \frac{v_{rel}}{c} \tag{1}$$

where v_{rel} is the relative transmitter-receiver motion (negative indicates motion towards each other, positive indicates motion away from each other), and c is the speed of sound in the UWA channel. In the time domain the effect of Doppler scaling on a signal is

$$r(t) = s\,(at) \tag{2}$$

where $r(t)$ is the received signal and $s(t)$ is the transmitted signal. While in the frequency domain

$$R(f) = \; S\left(\frac{f}{a}\right) \tag{3}$$

where $R(f)$ is the received signal and $S(f)$ is the transmitted signal in the frequency domain assuming the signal is normalised. In a UWA communication system the channel is modelled as a linear time invariant channel. The received signal is a superposition of multiple Doppler scaled, delayed, and attenuated copies of the transmitted signal. The received signal $r(t)$ at time t is given by

$$r(t) = \sum_{i=1}^{L} A_i s(a_i(t-\tau_i)) + n(t), \tag{4}$$

where $s(t)$ is the transmitted signal, i denotes path index, A_i is the attenuation, a_i is the Doppler scaling factor, τ_i is the delay, $n(t)$ is the noise signal, and L is the total number of paths. Unlike with common Doppler estimation, τ_i and a_i are statistically independent for all paths.

For estimating the UWA channel, the chirp signal is adopted as the pilot and is given by

$$x(t) = \Re\left\{e^{j(2\pi f_0 t + \pi k t^2 + \Phi_0)}\right\}, \qquad \forall t \in (t_0, t_1)\,. \tag{5}$$

where f_0 is the starting frequency of the signal, k is the chirp rate, Φ_0 is the initial phase, t_0 is the starting time, t_1 is the ending time, and $\Re\{\cdot\}$ is the real part.

III. The Fractional Fourier Transform

The FrFT of a function $x(t)$ with parameter ϕ is given by

$$X_\phi(u) = \int_{-\infty}^{\infty} x(t) K_\phi(t,u)\, dt$$

$$K_\phi(t,u) = \begin{cases} A_\phi e^{j\frac{t^2+u^2}{2}\cot\phi - jut\csc\phi}, & \text{for } \phi \neq n\pi \\ \delta(t-u), & \text{for } \phi = 2n\pi \\ \delta(t+u), & \text{for } \phi = (2n\pm 1)\pi \end{cases} \tag{6}$$

where u is the fractional Fourier domain variable. The FrFT is a generalised Fourier transform parameterised by ϕ, representing an angle of rotation in the time-frequency plane. The FrFT has a powerful geometric interpretation [8]. Consider a new set of axes on the time-frequency plane with u axis overlaid on the time axis and the v axis overlaid on the frequency axis. Suppose this new set of axes is then rotated anticlockwise by ϕ radians as depicted in the left side of Fig. 2 with the chirp

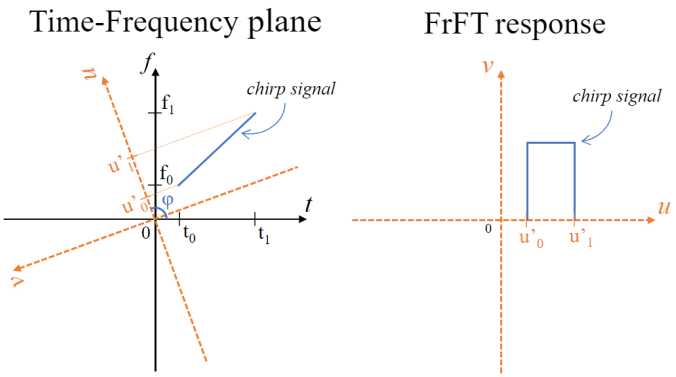

Fig. 2. Geometric interpretation of FrFT. Chirp signal on in the time-frequency plane (left). The FrFT response of the same signal (right)

as the signal under transformation. The FrFT response is then the projection of the signal onto the new set of axes shown in the right side of Fig. 2. Using Parseval's Theorem, which states the area under the signal in the time frequency domain is equal to the area in the FrFT domain, the height of the FrFT response can be determined [8]. By extending this geometric interpretation we can see that there exists a FrFT transform with a specific FrFT parameter, $\phi^\star$, for which a chirp signal transforms into a narrow delta peak. This occurs when the u axis is perpendicular to the gradient of the chirp as depicted in the left side of Fig. 3. The FrFT response is a narrow peak since the projection has a single point as the region of support as seen in the right side of Fig. 3. It can be shown that for every chirp rate k there exists one angle ϕ at which the response is a delta. For the remainder of this paper $\phi^\star$ will be referred to as the *optimal FrFT parameter*. Combining this with the fact that a one-to-one function relates Doppler scaling a to chirp rate k results in the important property that there exists a unique $\phi^\star$ for every Doppler scaling factor acting on a chirp signal.

This property is crucial in allowing the FrFT to extract the transmitted chirp from a superposition of delayed and scaled copies of the original signal. The discrete FrFT will be used to compute the discrete signals encountered in underwater

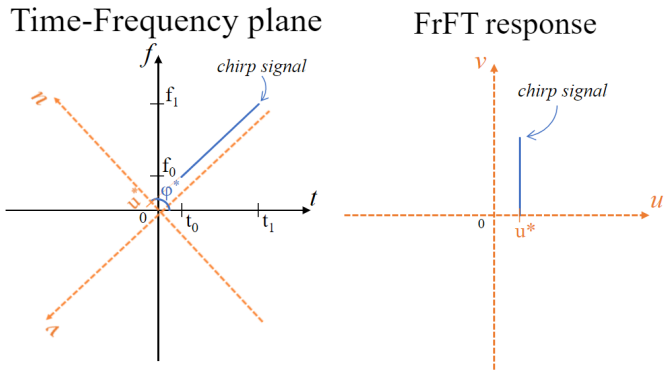

Fig. 3. The optimal FrFT transform in the time-frequency plane (left), which occurs when the u axis is perpendicular to the chirp signal. The delta peak response in the FrFT domain (right)

communications. It follows the same geometric interpretation as the continuous case outlined above. [9].

IV. Novel UWA Channel Estimation Algorithm

The novel estimation algorithm is presented in three sections: the creation of the $u-\phi$ image, applying key point detection, and computation of channel parameters.

A. Creation of $u-\phi$ image

Let N denote the number of FrFTs to be performed. N copies of the received signal are created and $\phi = \{\phi_0, \phi_1, ..., \phi_{N-1}\}$ are chosen to be equally spaced across predetermined start and end values. The ϕ range is theoretically bounded by 0 and π, however this range can be greatly reduced to improve computation speed given the typical velocities encountered in underwater environments. The discrete FrFT is then performed on each copy using each value from the ϕ range. Obtained responses are arranged in a $u-\phi$ 2D array such that the horizontal axis contains the ϕ value and the vertical axis contains the FrFT response. By storing the FrFT responses in such a way, the resulting 2D array, when viewed as an image, displays characteristic X-shapes. The presence of the X-shapes can be understood by considering a single chirp signal. Firstly, there exists a unique $\phi^\star$ determined by the chirp rate. As ϕ increases towards $\phi^\star$ the projection of the chirp onto the FrFT axes diminishes in region of support as the angle of the axes approaches the angle of the chirp signal. At the exact point $\phi = \phi^\star$ the response is narrowest. As ϕ increases past $\phi^\star$ the region of support expands at the same rate at which the region decreased due to the geometrical symmetry. By Parseval's theorem the height must increase as the region of support contracts and conversely, must decrease as the region of support expands. Fig. 4 illustrates this behaviour with the height of the surface representing the amplitude of the FrFT response.

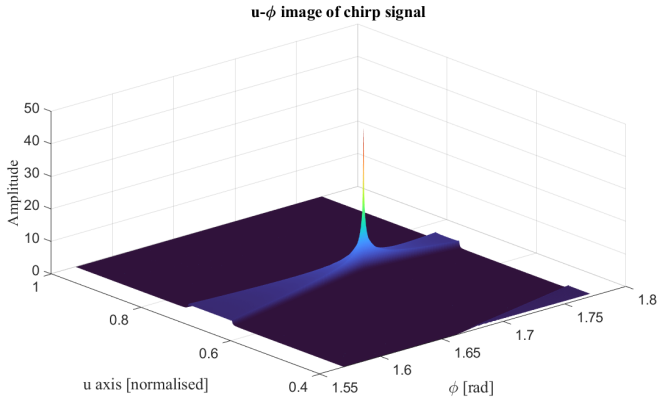

Fig. 4. 3D rendering of u-ϕ image. The region of support decreases as ϕ approaches $\phi^\star$ and then increases as ϕ recedes from $\phi^\star$. The height increases closer to $\phi^\star$ and drops further away

Delaying the chirp signal in time will not influence $\phi^\star$ but will change the angles of the X-shape wings and its position along the u-axis. Since the received signal is a superposition

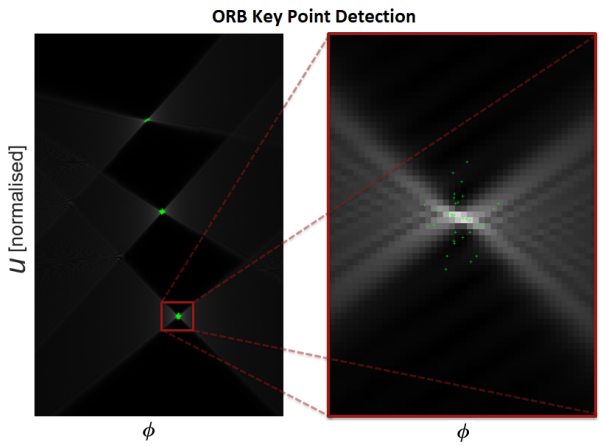

Fig. 5. Key points found by ORB algorithm (left). Points cluster around true crossing point and are averaged to improve accuracy (right).

of delayed and Doppler scaled copies of a chirp pilot, the $u-\phi$ image will similarly be a superposition of X-shapes. The left side of Fig. 5 shows the 2D array depicted as an image with lighter pixels denoting higher magnitude responses. Each X-shape corresponds to a multipath with different Doppler scaling and delay values, the X-shapes and crossing points are accordingly different. The next step is to extract these crossing point location co-ordinates.

B. Applying Key Point Detection

Our proposed method applies a key point detection algorithm to extract the co-ordinates of each crossing point. Key point detection is a widely used image processing tool which identifies distinct points in images or video frames [10]. The most commonly used algorithms were tested and compared to each other and based on estimation error the Orientated FAST and Rotated BRIEF (ORB) algorithm was chosen. The ORB algorithm is based on the Features from Accelerated Segment Test (FAST) algorithm. It evaluates whether a pixel is a key point or not based on the 16 pixels forming a Bresenham circle of radius 3 around it, shown in Fig. 6. Suppose the pixel has intensity is represented by a positive real number, I_p and an appropriate threshold, I_t is selected. If there exists m contiguous pixels in the circle that are all brighter than $I_p + I_t$ or are all darker than $I_p - I_t$ then the centre pixel is a key point. The FAST algorithm works best when $12 \leq m \leq 16$. Full details of the ORB and FAST algorithms can be found in [11]. The number of key points to be found can be specified as an input parameter. The simulation in this paper uses a 2D array as the input to ORB and the output is the specified number of co-ordinate pairs.

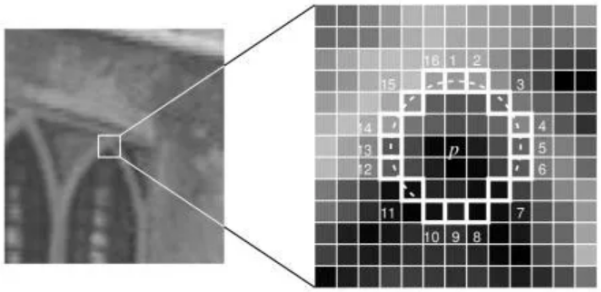

Fig. 6. The Bresenham circle of pixels under consideration to determine the key pint status of the centre pixel

C. Computation of channel parameters

An excess of key points are found so clusters around crossing points can be averaged. The averaging process improves efficiency since ORB is rotationally invariant hence key points will be spread evenly in the horizontal and vertical directions. The equal spread in both directions can be seen in the right side of Fig. 5. The number of key points is also chosen so that non-crossing point features are not included. Identified key points are then grouped together if their separation is below a threshold distance. This threshold distance is carefully chosen to include all key points comprising a cluster but exclude neighbouring key points and outliers. Fig. 7 shows a suitably chosen threshold distance. All points within each group are averaged to find the co-ordinates of each crossing point, $(u_p^\star, \phi_p^\star)$. Lastly, channel Doppler scaling, $\hat{a}_p$ and multipath delay, $\hat{\tau}_p$ for path p can then be obtained as shown below.

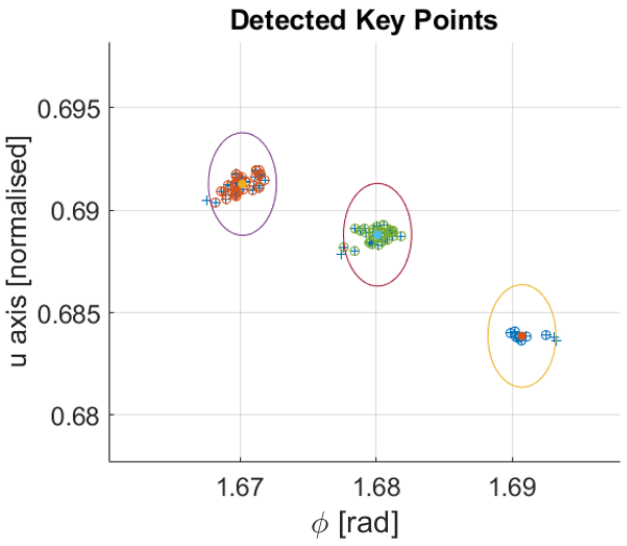

Fig. 7. Key points are grouped using a distance threshold. Threshold also allows falsely detected points to be ignored. Circles represent the threshold distance

Consider the case when $\phi = \phi_\star$ as shown in Fig. 8.

For simplicity, let $t_0^{'} = 0$. In Fig. 8 $f_0^{'}$ is the received chirp starting frequency, τ is the multipath delay, and $k^{'}$ is the received chirp rate. The triangle enclosed by the vertices A, E, and O is denoted $\triangle AEO$ and the triangle enclosed by vertices A, B, and C is denoted $\triangle ABC$. $\angle EAO$ denotes the angle of vertex A, while $\angle AOE$ denotes the angle of vertex

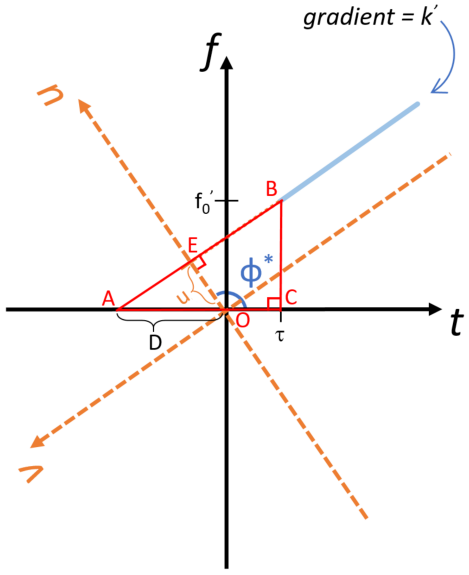

Fig. 8. Derivation of channel parameter formulae

E within $\triangle AEO$.
In $\triangle AEO$, $\angle EAO = \phi^\star - \frac{\pi}{2}$. In $\triangle ABC$:

$$\tan\left(\phi^\star - \frac{\pi}{2}\right) = \frac{f_0^{'}}{D+\tau} \quad , \tag{7}$$

In $\triangle AEO$, $\angle AOE = \pi - \phi^\star$, so

$$\cos\left(\pi - \phi^\star\right) = \frac{u}{D} \quad . \tag{8}$$

Solving (7) and (8) for D, we have

$$D = \frac{u}{\cos\left(\pi - \phi^\star\right)} = \frac{f_0^{'}}{\tan\left(\phi^\star - \frac{\pi}{2}\right)} - \tau \quad . \tag{9}$$

Using the identities, $\cos(\pi - x) = -\cos(x)$, and $\tan(x - \frac{\pi}{2}) = -\cot(x)$, (9) reduces to

$$\frac{u}{-\cos\phi^\star} = \frac{f_0^{'}}{-\cot\phi^\star} - \tau \quad , \tag{10}$$

and rewriting $\cot\phi^\star$ as $\cos\phi^\star \,/\, \sin\phi^\star$ gives

$$\frac{u}{\cos\phi^\star} = \frac{f_0^{'}\sin\phi^\star}{\cos\phi^\star} + \tau \quad , \tag{11}$$

then subjecting u results in:

$$u = f_0^{'}\sin\phi^\star + \tau\cos\phi^\star \quad . \tag{12}$$

The received chirp has been acted on by a single Doppler factor, a, thus: $f_0^{'} = af_0$. Since all signals are discrete the frequency and time quantities must be normalised by using

$$f_0 \rightarrow \frac{f_0}{F_{samp}} \quad , \tag{13a}$$

$$\tau \rightarrow \frac{\tau}{T_{sig}} \quad , \tag{13b}$$

where F_{samp} is sampling frequency, and T_{sig} is pilot duration. Substituting these normalisation factors and then rearranging for τ results in

$$\tau = \left(\frac{u - \left(\frac{af_0}{F_{samp}}\right)\sin\phi^\star}{\cos\phi^\star}\right) T_{sig} \quad . \tag{14}$$

The derivation for Doppler scaling factor, a is much simpler. The optimal FrFT occurs when $\phi^\star$ is perpendicular to the chirp gradient, as shown in Fig. 8, and is given by

$$\phi^\star = -\tan^{-1}\left(\frac{1}{k^{'}}\right) \quad . \tag{15}$$

The received chirp rate and transmitted chirp rate is related by

$$k^{'} = a^2 k \quad . \tag{16}$$

Again normalisation is required for discrete signals

$$k \rightarrow k\frac{T_{sig}}{F_{samp}} \quad . \tag{17}$$

Substituting and rearranging for a results in

$$a = \sqrt{-\cot\phi\left(\frac{F_{samp}}{kT_{sig}}\right)} \quad . \tag{18}$$

Combing equation (14) and (18) allows the direct computation of the channel parameters Doppler scaling and multipath delay from the crossign point co-ordinates $(u_p^\star, \phi_p^\star)$

$$\hat{a}_p = \sqrt{-\cot(\phi_p^\star)\left(\frac{F_{samp}}{kT_{sig}}\right)} \quad , \tag{19a}$$

$$\hat{\tau}_p = \left(\frac{u_p^\star - \left(\frac{\hat{a}_p f_0}{F_{samp}}\right)\sin\phi_p^\star}{\cos\phi_p^\star}\right) T_{sig} \quad , \tag{19b}$$

where p denotes the multipath index.

Existing FrFT-based methods use only the ϕ coordinate to calculate Doppler [7]. At the same time, an additional correlation procedure obtains delay. With the proposed approach, greater efficiency is achieved since subtracting the dominant path and iterative computation is avoided [7].

Furthermore, performance of the overall method depends on the accuracy of ORB which in turn is directly proportional to the sample length of the received signal and the number of FrFTs used in the scan. Thus higher accuracy can be obtained by increasing the number of FrFTs.

V. Validation, Results, and Conclusions

We simulated the proposed method in a UWA channel consisting of 7 multipaths with Doppler scaling ranging from 0.95 to 1.05 following a normal distribution while the time delay ranges from 0 to 0.2 seconds following a Rayleigh distribution. Results of the simulation performed in MATLAB show successful estimation of channel parameters: Doppler scaling and multipath delay. The number of FrFTs was set

to 1000 as further increase produced diminishing returns in accuracy. ϕ ranged from 1.57 to 1.7 with equally spaced steps and a total of 1000 points. Starting and ending values were chosen to include all major X-shape features. The number of key points was determined to be 90 since any further increase included non-crossing point features as key points. From Fig. 9 we see that the maximum percentage error for Doppler scaling is 0.1% while the maximum error for delay is within 2ms. The number of multipaths to be estimated is set to 7. Note that the detection accuracy depends on the number of FrFTs used, so a trade-off exists between precision and computational speed.

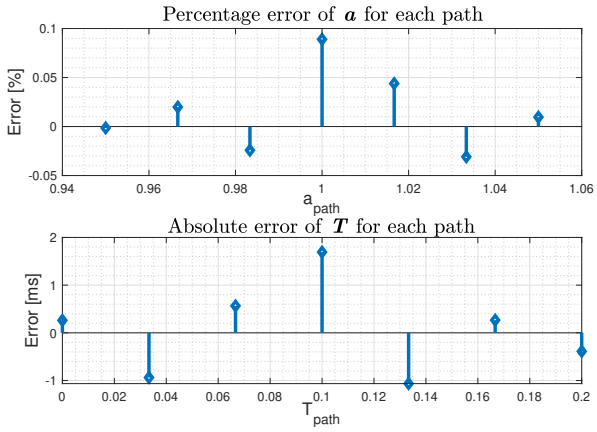

Fig. 9. Error statistics from 7 path simulation. a_{path} denotes the Doppler scale factor per path. T_{path} denotes the delay per path

This paper proposes a new channel estimation algorithm for UWA systems that utilises FrFTs and key point detection. Our approach jointly estimates Doppler and multipath delay for all multipaths simultaneously. Simulations results show a 0.1% Doppler scaling estimation accuracy and a $\pm 2ms$ error for multipath delay. While our algorithm has improved performance and efficiency, further enhancements can be made by refining the key point detection algorithm and conducting a more in-depth analysis of error statistics.

REFERENCES

[1] M. Stojanovic and J. Preisig, "Underwater acoustic communication channels: Propagation models and statistical characterization," *IEEE Communications Magazine*, vol. 47, no. 1, pp. 84–89, 1 2009.

[2] A. V. Gadagkar and B. R. Chandavarkar, "A Comprehensive Review on Wireless Technologies and their Issues with Underwater Communications," in *2021 12th International Conference on Computing Communication and Networking Technologies (ICCCNT)*. IEEE, 7 2021, pp. 1–6.

[3] A. Palmeiro, M. Martin, I. Crowther, and M. Rhodes, "Underwater radio frequency communications," in *OCEANS 2011 IEEE - Spain*. IEEE, 6 2011, pp. 1–8.

[4] Ye Jiang and A. Papandreou-Suppappola, "Discrete time-scale characterization of wideband time-varying systems," *IEEE Transactions on Signal Processing*, vol. 54, no. 4, pp. 1364–1375, 4 2006.

[5] Baosheng Li, Shengli Zhou, M. Stojanovic, L. Freitag, and P. Willett, "Multicarrier Communication Over Underwater Acoustic Channels With Nonuniform Doppler Shifts," *IEEE Journal of Oceanic Engineering*, vol. 33, no. 2, pp. 198–209, 4 2008.

[6] M. Stojanovic, "Low Complexity OFDM Detector for Underwater Acoustic Channels," in *OCEANS 2006*. IEEE, 9 2006, pp. 1–6.

[7] Y. Zhao, H. Yu, G. Wei, F. Ji, and F. Chen, "Parameter Estimation of Wideband Underwater Acoustic Multipath Channels based on Fractional Fourier Transform," *IEEE Transactions on Signal Processing*, vol. 64, no. 20, pp. 5396–5408, 10 2016.

[8] L. B. Almeida, "The fractional Fourier transform and time-frequency representations," *IEEE Transactions on Signal Processing*, vol. 42, no. 11, pp. 3084–3091, 1994.

[9] H. Ozaktas, O. Arikan, M. Kutay, and G. Bozdagt, "Digital computation of the fractional Fourier transform," *IEEE Transactions on Signal Processing*, vol. 44, no. 9, pp. 2141–2150, 9 1996.

[10] Analytics Vidhya, "Computer Vision — Feature Detection and Matching," 3 2020.

[11] E. Rublee, V. Rabaud, K. Konolige, and G. Bradski, "ORB: An efficient alternative to SIFT or SURF," in *2011 International Conference on Computer Vision*, 2011, pp. 2564–2571.